Granular Matter (2011) 13:643–656
DOI 10.1007/s10035-011-0277-0

ORIGINAL PAPER

# Benchmark tests for verifying discrete element modelling codes at particle impact level

**Y. C. Chung · J. Y. Ooi**

Received: 30 September 2010 / Published online: 5 July 2011


**Abstract** Over the past 30 years, the Discrete Element Method (DEM) has rapidly gained popularity as a tool for modelling the behaviour of granular assemblies and is being used extensively in both scientific and industrial applications. However, it is far from clear from reviewing the literature whether the large number of DEM codes have been verified and checked against fundamental benchmark problems. DEM simulates the dynamics of each particle in an assembly by calculating the acceleration resulting from all the contact forces and body forces. It is clearly necessary that such a model be validated or verified by comparing with experimental results, analytical solutions or other numerical results (e.g. Finite Element Analysis (FEA) results) at particle impact level. There appears to be no standard benchmark tests against which DEM codes can be verified. It is thus essential and useful to establish a set of standard benchmark tests to confirm that these DEM codes are modelling the particle dynamics as intended. This paper proposes a set of benchmark tests to verify DEM codes at particle impact level for spherical particles. The analytical solutions derived from elasticity theory for elastic normal collision of two spheres or a sphere with a rigid plane are first reviewed. These analytical solutions apply only to the elastic regime for normal impact. Secondly, the analytical solutions of frictional oblique impact between two spheres or a sphere with a rigid plane are scrutinized and derived. These analytical solutions originate from the dynamics principles and should be satisfied for any DEM contact force model with prescribed friction and restitution coefficients. A set of eight benchmark tests are designed and performed using commercial DEM codes. Test 1 and Test 2 consider the elastic normal impact of two spheres or a sphere with a rigid plane, whereas the other tests (Test 3–Test 8) investigate the energy dissipation due to the collision. These benchmark tests also involve different types of material. The DEM results were compared with the analytical solutions, experimental or FEA results found in the literature. All benchmark tests showed good to excellent match, providing a quantitative verification for the codes used in this study. These benchmark tests not only verify DEM codes but also enhance the understanding of fundamental impact phenomena for modelling a large number of particles.

**Keywords** Discrete element method · Calibration and verification · Benchmark test · Spherical system · Normal impact · Frictional oblique impact

Y. C. Chung (✉)
Department of Computer Science and Information Engineering, Nanya Institute of Technology, Jhongli 32091, Taiwan, ROC
e-mail: chung@nanya.edu.tw; yunchichung123@yahoo.com.tw

J. Y. Ooi
Institute for Infrastructure and Environment, School of Engineering, University of Edinburgh, Edinburgh EH9 3JN, UK

## 1 Introduction

The Discrete Element Method (DEM) [1] is by now a well-established method for modelling the dynamic behaviour of granular assemblies subjected to a variety of loading scenarios. Over the past thirty years, the method has rapidly gained popularity as a modelling tool for granular mechanics problems and has been used extensively in both scientific and industrial applications (e.g. silo flow: Zhu et al. [2], Ketterhagen et al. [3], Tao et al. [4], ball mill process: Kwan et al. [5], Yang et al. [6], Cleary et al. [7], two-phase flow: Müller et al. [8], Chu et al. [9], Maio et al. [10], vibrated beds: Lu and Hsiau [11], Majid and Walzel [12], Naeini and Spelt [13], others: Luding [14], Härtl and Ooi [15], Chung and Ooi [16]). However, it is far from clear when

reviewing the literature whether the large number of DEM codes that are being used around the world have been verified and checked against fundamental benchmark problems. Holst et al. [17,18] reported major discrepancies between the predictions of different DEM codes around the world when performing blind calculations of the same tightly defined problem. DEM simulates the dynamics of each particle in an assembly by calculating the acceleration resulting from all the contact forces and body forces. It is clearly necessary that where possible, each DEM code is validated or verified by comparing with experimental results, analytical solutions or other numerical results (e.g. Finite Element Analysis (FEA) results) at particle impact level. There appears to be no standard benchmark tests against which DEM codes can be verified.

Timoshenko and Goodier [19] presented the analytical solution of elastic normal impact of two spheres, which was derived from Hertz theory [20] and elasticity theory. Maw et al. [21] presented an analytical solution for an oblique impact of a homogeneous elastic sphere on a rigid half-space. Their solution was based on Hertz theory [20] for normal contact, and Mindlin and Deresiewicz theory [22] for tangential elastic frictional contact. Vu-Quoc et al. [23] conducted FEA of frictional elasto-plastic contact for two spherical particles. They reported the collision properties in the normal and tangential directions of the contacting spheres, including force-displacement (FD) curves, contact stresses, contact-area radius and contact curvature. Zhang and Vu-Quoc [24] further modelled the dynamic process of normal collision between a deformable sphere and a frictionless rigid planar surface using the same FEA. The restitution coefficient was predicted as a function of the incoming velocity in elasto-plastic collision. The relationships among the restitution coefficient, incoming velocity, contact FD curve, contact duration and normal pressure distribution in contact area were also reported. Wu et al. [25] also performed finite element analyses of both elastic and elasto-plastic oblique impacts of a sphere with a target wall. For elastic oblique impacts, the results are in complete agreement with previous study. However, for elasto-plastic oblique impacts, the normal coefficient of restitution is not only a function of the normal impact velocity, but also depends on the impact angle. Based on the study of normal and frictional elasto-plastic FEA [23,24], Vu-Quoc et al. proposed a series of FD models [26–28] at particle impact level. An elasto-plastic normal FD model in displacement-driven version [26] was established to account for plastic deformation of two contacting spheres. The elasto-plastic frictional tangential FD models in force-driven and displacement-driven versions [27,28], which are consistent with the elasto-plastic normal FD model [26], were then developed to account for both elastic and plastic deformation together with interfacial friction in collision of spheres. A principal feature of these FD models is the additive decomposition of the radius of the elasto-plastic contact area into an elastic part and a plastic part. Foerster et al. [29] performed experiments by dropping small spheres in free fall without initial spin. They measured the impact properties of these small spheres in binary collision or in collision with a flat surface, and demonstrated that their simple model, based on Coulomb friction coefficient, normal restitution coefficient and tangential restitution coefficient, can capture the impact behaviour over a wide range of incident angles. Kharaz et al. [30] also conducted a drop test for aluminium oxide spheres impacting a thick soda-lime glass anvil over impact angles from normal to very near glancing incidence and calculated the normal and tangential restitution coefficients. The experimental results were compared with the simple theoretical model and numerical results of Maw et al. Plantard and Papini [31] carried out polymer particle tests, which gave the measurement of the contact force and displacement and the measurement of the electric resistance, to investigate the mechanical and electric properties of the polymer particulate system. The elasto-plastic normal FD model by Vu-Quoc [26] was adopted and carefully validated against the corresponding experiments using scanning electron microscopy (SEM) and atomic force microscopy (AFM). Their experimental results were shown to be in line with Vu-Quoc's model and the theories of contact mechanics. The results of these studies described above can be used to compare with the DEM benchmark tests at particle impact level.

This paper presents a set of simple benchmark tests for checking the validity of DEM codes at particle impact level and ensuring that these DEM codes are modelling the particle dynamics as intended. These benchmark tests concentrate solely on spherical systems. The analytical solutions obtained from elasticity theory for elastic normal impact between two spheres or a sphere with a rigid plane are first reviewed. These solutions do not take into account plastic deformation of contacting spheres during contact process (i.e. no energy dissipation). The analytical solutions for frictional oblique impact of two spheres or a sphere with a rigid plane are then comprehensively examined and derived. The restitution coefficient is assumed to be a constant in the mathematical model although it is known to be a function of incoming velocity. These analytical solutions come from the dynamics principles and should be suitable for any DEM contact force model (frictional visco-elastic [1,32] or frictional elasto-plastic contact force model [27,28]) and any material type once the friction coefficient and restitution coefficient are defined. Finally, a set of eight benchmark tests are described and subsequently conducted using the commercial DEM software PFC3D [33] or EDEM [34]. Test 1 and Test 2 verify the elastic normal impact (i.e. the value of the restitution coefficient is unity), Test 3 verifies the energy dissipation for normal impact, and the other tests (Test 4–Test 8) examine the energy dissipation

due to the oblique collision of two spheres or a sphere with a rigid plane. Several materials were used in these benchmark tests. The background and results of these benchmark tests are presented and discussed in this paper.

## 2 Analytical solutions for elastic normal impact and frictional oblique impact

Before simulating a granular solid that comprises many particles involving multiple collisions, it is useful to examine the fundamental phenomena for each impact. These include elastic normal impact and frictional oblique impact of two spheres or a sphere with a rigid plane. The problem of elastic normal impact of two spheres was presented in Timoshenko and Goodier [19] and has been used numerous times before to verify the normal force calculation in DEM (e.g. [35,36]). The problem of hard-sphere collision with frictional contact was proposed by Vu-Quoc and Zhang [37] to verify the tangential force calculation. The dynamics principles [38] are elaborated here to examine more thoroughly the frictional oblique impact of two spheres or a sphere with a rigid plane. These are outlined below to provide the key elements for these solutions.

For two identical elastic spheres impacting with incoming velocities $V_1$ and $V_2$, the force-displacement relation during the collision can be described using Hertz contact theory. The complete solution for the elastic normal impact can be found in Timoshenko and Goodier [19] and will not be repeated here. The duration of the collision $T$ is given by (1).

$$T = 2.943 \left[ \frac{5\sqrt{2}}{4} \frac{\pi\rho\left(1-\nu^2\right)}{E} \right]^{\frac{2}{5}} \frac{r}{V_{\text{rela}}^{1/5}} \tag{1}$$

where $E$ is the Young's modulus, $\nu$ is the Poisson's ratio, $\rho$ is the density, $r$ is the radius and $V_{rela}(=V_1+V_2)$ is the relative velocity of the two spheres. The maximum normal contact displacement and force are given by (2) and (3) respectively.

$$\alpha_{\max} = \left[ \frac{5\sqrt{2}}{4} \frac{\pi\rho\left(1-\nu^2\right)}{E} \right]^{\frac{2}{5}} r V_{\text{rela}}^{\frac{4}{5}} \tag{2}$$

$$P_{\max} = \left[ \frac{2}{9} \frac{rE^2}{\left(1-\nu^2\right)^2} \right]^{\frac{1}{2}} \alpha_{\max}^{\frac{3}{2}} \tag{3}$$

Equations 1–3 are also applicable to the case where a sphere impacts a rigid planar surface normally, which is equivalent to two identical spheres colliding with the same magnitude and opposite direction of velocity. Therefore, for a sphere impacting on a rigid plane with incoming velocity $V_1$, the contact duration, maximum normal contact displacement and force can be obtained by replacing $V_{\text{rela}}$ with $2V_1$ and knowing that the maximum normal contact displacement is half the value from (2). It should be noted that (1–3) are restricted to the elastic regime since these analytical solutions do not consider plastic deformation of contacting spheres during the contact process.

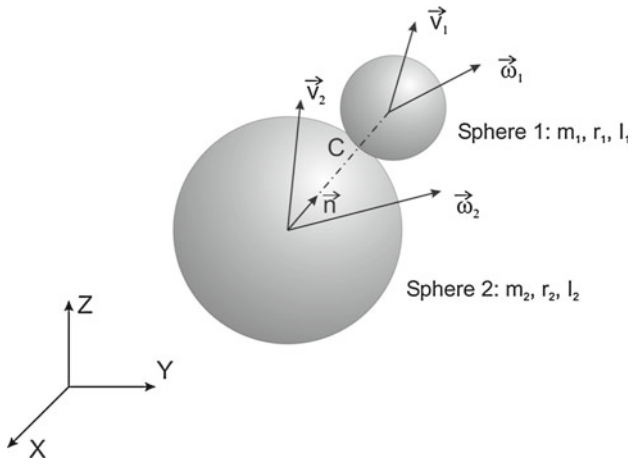


**Fig. 1** A schematic of two colliding spheres in a 3D Cartesian coordinate system

Consider an oblique impact between two spheres in a 3D space, as illustrated in Fig. 1: $m_1$ and $m_2$ denote the masses of Sphere 1 and Sphere 2, $r_1$ and $r_2$ the radii, and $I_1$ and $I_2$ the mass moments of inertia of these spheres about their mass centres; $\vec{V}_1$ and $\vec{V}_2$ denote the pre-collision linear velocities at their mass centres, and $\vec{\omega}_1$ and $\vec{\omega}_2$ the pre-collision angular velocities of these spheres, respectively. The two spheres collide at the contact point C. The relative velocity of Sphere 1 with respect to Sphere 2 at the contact point is given by (4).

$$\vec{V}_{cp,21} = \vec{V}_1 - \vec{V}_2 - \vec{\omega}_1 \times r_1\vec{n} - \vec{\omega}_2 \times r_2\vec{n} \tag{4}$$

where $\vec{n}$ is the unit normal vector joining the centres of Sphere 1 and Sphere 2. The unit normal vector $\vec{\lambda}$ of the plane where the normal and tangential contact forces occur can be expressed as (5).

$$\vec{\lambda} = \frac{\vec{V}_{cp,21} \times \vec{n}}{\left|\vec{V}_{cp,21} \times \vec{n}\right|} \tag{5}$$

The unit vector for the tangential direction can then be expressed as (6).

$$\vec{t} = \vec{n} \times \vec{\lambda} \tag{6}$$

An orthogonal coordinate system, based on the three unit vectors $\vec{t}$, $\vec{n}$ and $\vec{\lambda}$, can be established, as shown in Fig. 2. The linear and angular velocities immediately before and after impact can be decomposed into components along the $\vec{t}$, $\vec{n}$ and $\vec{\lambda}$ directions using coordinate transformation. Figure 2 also depicts the pre-collision and post-collision linear and angular velocities. For Sphere 1, $V_{cn,1}$ and $V_{ct,1}$ denote the pre-collision normal and tangential velocities at its mass

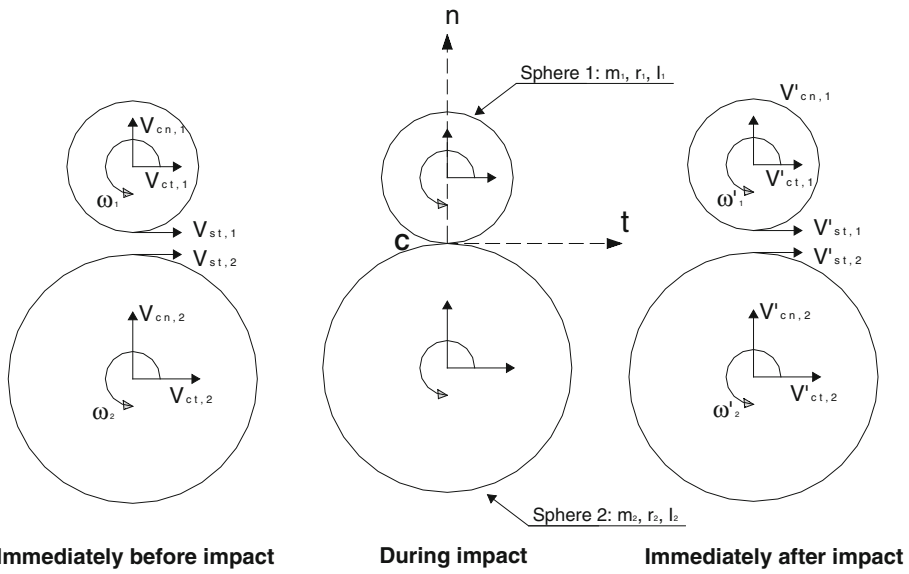


**Fig. 2** Linear and angular velocities before and after impact in an orthogonal coordinate system based on $\vec{t}$, $\vec{n}$ and $\vec{\lambda}$

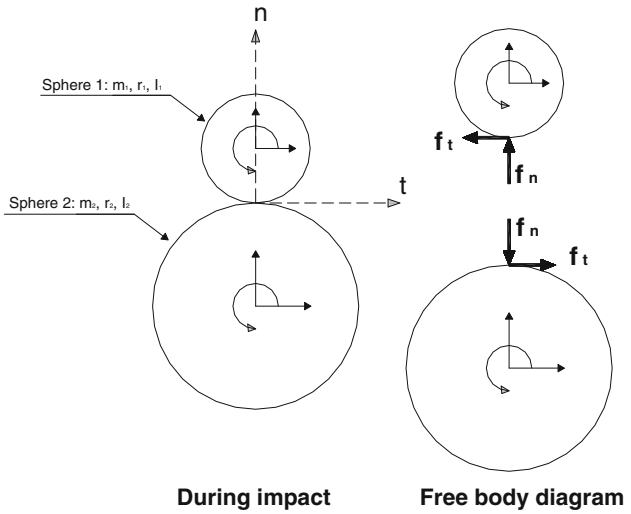


**Fig. 3** Normal and tangential contact forces during impact

centre, $V_{st,1}$ the pre-collision tangential velocity at the contact point and $\omega_1$ the pre-collision angular velocity, whilst $V'_{cn,1}$, $V'_{ct,1}$, $V'_{st,1}$ and $\omega'_1$ denote the corresponding post-collision values. Similar notations also apply to Sphere 2.

Figure 3 illustrates the normal contact force $f_n$ and tangential contact force $f_t$ in a free-body diagram during impact. Applying the linear and angular impulse-momentum principles to Sphere 1, three impulse-momentum equations can be expressed as (7–9).

$$F_t = -m_1\left(V'_{ct,1} - V_{ct,1}\right) \tag{7}$$
$$F_n = m_1\left(V'_{cn,1} - V_{cn,1}\right) \tag{8}$$
$$r_1 F_t = -I_1\left(\omega'_1 - \omega_1\right) \tag{9}$$

where $F_n$ is the normal linear impulse and is expressed as $F_n = \int_0^T f_n dt$; $F_t$ is the tangential linear impulse and is expressed as $F_t = \int_0^T f_t dt$; $T$ is the contact duration. Similarly, another three impulse-momentum equations for Sphere 2 can be written as (10–12).

$$F_t = m_2\left(V'_{ct,2} - V_{ct,2}\right) \tag{10}$$
$$F_n = -m_2\left(V'_{cn,2} - V_{cn,2}\right) \tag{11}$$
$$r_2 F_t = -I_2\left(\omega'_2 - \omega_2\right) \tag{12}$$

The relative normal velocities immediately before and after impact can be expressed in (13). The relative tangential velocities immediately before and after impact at the mass centre and at the contact point can be respectively expressed in (14) and (15).

$$V_{cn} = V_{cn,1} - V_{cn,2};\ V'_{cn} = V'_{cn,1} - V'_{cn,2} \tag{13}$$
$$V_{ct} = V_{ct,1} - V_{ct,2};\ V'_{ct} = V'_{ct,1} - V'_{ct,2} \tag{14}$$
$$V_{st} = V_{st,1} - V_{st,2};\ V'_{st} = V'_{st,1} - V'_{st,2} \tag{15}$$

The relationships between the tangential velocities at the contact point and those at the mass centre can be written as (16) and (17).

$$V_{st,1} = V_{ct,1} + r_1\omega_1;\ V_{st,2} = V_{ct,2} - r_2\omega_2 \tag{16}$$
$$V'_{st,1} = V'_{ct,1} + r_1\omega'_1;\ V'_{st,2} = V'_{ct,2} - r_2\omega'_2 \tag{17}$$

The normal restitution coefficient and tangential restitution coefficients based on the mass centre and contact point are defined respectively as (18).

$$e_n = -\frac{V'_{cn}}{V_{cn}};\ e_t = \frac{V'_{ct}}{V_{ct}};\ \beta = -\frac{V'_{st}}{V_{st}} \tag{18}$$

In the following derivation, the tangential force, $f_t$, is always opposite to the relative pre-collision tangential velocity at the contact point, $V_{st}$. Equating the normal linear impulse $F_n$ in (8) and (11) and using the expressions in (13) and (18) ($e_n$) yield (19).

$$F_n = -\frac{m_1 m_2}{m_1 + m_2}(1 + e_n)\, V_{cn} \tag{19}$$

Similarly, combining (7, 10, 14 and 18 ($e_t$)) yields (20).

$$F_t = \frac{m_1 m_2}{m_1 + m_2}(1 - e_t)\, V_{ct} \tag{20}$$

Combining (7, 10, 16 and 17) together with (15) and (18) ($\beta$) further yields (21).

$$F_t = \frac{m_1 m_2}{m_1 + m_2}\left[(1 + \beta)\, V_{st} + r_1(\omega_1' - \omega_1) + r_2(\omega_2' - \omega_2)\right] \tag{21}$$

The oblique impact of a hard sphere can result in either a sliding regime or a sticking regime. Each may arise depending on the contact friction and the incident angle at the contact point which is given by $\tan^{-1}(|V_{st}| / |V_{cn}|)$. The relationship between the normal contact force $f_n$ and tangential contact force $f_t$ during collision must follow (22).

$$|f_t| \leq \mu\ f_n \tag{22}$$

where $\mu$ is the friction coefficient between the two spheres. The two cases of sliding collision and sticking collision can be considered as follows: (1) sliding regime: the two spheres slide at the contact point during collision, thus satisfying the Coulomb friction law, that is, the "equal" sign holds; (2) sticking regime: for no sliding between the two spheres, the "less" sign holds. It should be noted that for the following inequalities "$\leq$", the "equal" sign represents sliding regime, whilst the "less" sign represents sticking regime. Equation 22 is also equivalent to (23).

$$|F_t| \leq \mu\ F_n \tag{23}$$

Substituting (19) and (20) into (23), the relationship between $e_t, e_n, \mu$ and $\frac{V_{ct}}{V_{cn}}$ can be derived as (24).

$$0 \leq (1 - e_t)\frac{V_{ct}}{V_{cn}} + \mu\,(1 + e_n) \tag{24}$$

Combining (9) and (12) into (21) and replacing $I_1$ and $I_2$ with $\frac{2}{5}m_1 r_1^2$ and $\frac{2}{5}m_2 r_2^2$ respectively result in (25).

$$F_t = \frac{2}{7}\frac{m_1 m_2}{m_1 + m_2}(1 + \beta)\, V_{st} \tag{25}$$

Substituting (19) and (25) into (23), the relationship between $\beta, e_n, \mu$ and $\frac{V_{st}}{V_{cn}}$ can be derived as (26).

$$0 \leq \frac{2}{7}\frac{(1 + \beta)}{(1 + e_n)}\frac{V_{st}}{V_{cn}} + \mu \tag{26}$$

Equations 24 and 26 indicate that once the normal restitution coefficient $e_n$, friction coefficient $\mu$ and pre-collision velocities are given, the tangential restitution coefficients $(e_t, \beta)$ can be determined. The relationship between $e_t$ and $\beta$ can also be determined as (27) by combining (20) with (25).

$$(1 - e_t)\, V_{ct} = \frac{2}{7}(1 + \beta) V_{st} \tag{27}$$

Recalling (18) for $\beta$, (26) can be rearranged and expressed as

$$-\frac{V_{st}'}{V_{cn}'} \leq \frac{7}{2}\mu(1 + \frac{1}{e_n}) + \frac{1}{e_n}\frac{V_{st}}{V_{cn}} \tag{28}$$

The above equation describes the relationship between the tangent of incident angle $\left(\frac{V_{st}}{V_{cn}}\right)$ and the tangent of recoil angle $\left(\frac{V_{st}'}{V_{cn}'}\right)$.

Equations 7–28 can be applied to the case where a sphere obliquely impacts on a rigid plane by deleting the physical quantities related to Sphere 2. The above equations will be used in the benchmark testing in the next section. It should be noted that any contact force model (frictional visco-elastic [1,32] or frictional elasto-plastic contact force model [27,28]) should comply with (24–28) since they are derived from the dynamics principles and only relate the pre-collision velocities to the post-collision velocities regardless of the contact process. Different contact force models however may have different critical incident angles that distinguish between sliding and sticking regimes, and may show different behaviours in the sticking regime.

## 3 Benchmark tests

A set of eight benchmark tests is designed and proposed to verify DEM codes for spherical contact, as outlined in Table 1. Test 1 and Test 2 (Timoshenko and Goodier [19], Zhang and Vu-Quoc [24]) verify the elastic normal contact of two identical spheres and of a sphere with a rigid plane. Test 3 (Ning and Ghadiri [39]) verifies the effect of restitution coefficient on normal impact. Test 4 (Foerster et al. [29], Kharaz et al. [30], Renzo and Maio [40]), Test 5 (Maw et al. [21], Wu et al. [25]) and Test 6 (Vu-Quoc and Zhang [37]) are employed to check the oblique impact between a sphere and a rigid plane. Test 7 and Test 8 (Chung [35]) are devised to check the oblique impact between two spheres.

The use of these benchmark tests is demonstrated here by verifying the PFC3D and EDEM commercial codes. The description of the DEM method or the PFC3D and EDEM codes can be found elsewhere (e.g. [1,33–35]) and will not be elaborated here. The two leading commercial DEM codes, PFC3D and EDEM, do not have built-in elasto-plastic contact force model. In this paper, the simplified Hertz–Mindlin contact model (HM visco-elastic contact force model) [32], which is equipped with a non-linear spring, a non-linear damper and a frictional slider in the tangential direction as well as a non-linear spring and a non-linear damper in the normal direction, was adopted for all benchmark tests. The required parameters for this contact force model are Young's modulus, Poisson's ratio, friction coefficient and coefficient of restitution. Energy is dissipated through contact friction

**Table 1** Summary of benchmark test problems

| Test no. | Title | Objective | Reference |
|---|---|---|---|
| 1 | Elastic normal impact of two identical spheres | Check the elastic normal contact between two spheres | Timoshenko and Goodier [19] |
| 2 | Elastic normal impact of a sphere with a rigid plane | Check the elastic normal contact between a sphere and a plane | Timoshenko and Goodier [19], Zhang and Vu-Quoc [24] |
| 3 | Normal contact with different restitution coefficients | Check the effect of damping ratio | Ning and Ghadiri [39] |
| 4 | Oblique impact of a sphere with a rigid plane with a constant resultant velocity but at different incident angles | Check the tangential force calculation between a sphere and a plane | Foerster et al. [29], Kharaz et al. [30], Renzo and Maio [40] |
| 5 | Oblique impact of a sphere with a rigid plane with a constant normal velocity but at different tangential velocities | Check the tangential force calculation between a sphere and a plane | Maw et al. [21], Wu et al. [25] |
| 6 | Impact of a sphere with a rigid plane with a constant normal velocity but at different angular velocities | Check the tangential force calculation between a sphere and a plane | Vu-Quoc and Zhang [37] |
| 7 | Impact of two identical spheres with a constant normal velocity and varying angular velocities | Check the tangential force calculation between two spheres | Chung [35] |
| 8 | Impact of two differently sized spheres with a constant normal velocity and varying angular velocities | Check the tangential force calculation between two spheres | Chung [35] |

**Table 2** DEM input parameters of benchmark tests

| Input parameters | Test No.1 | | Test No.2 | | Test No.3 | | Test No.4 | |
|---|---|---|---|---|---|---|---|---|
| | Ex. 1 | Ex. 2 | Ex. 1 | Ex. 2 | Ex. 1 | Ex. 2 | Ex. 1 | Ex. 2 |
| | Glass | Limestone | Al. alloy | Mg. alloy | Al. oxide | Cast iron | Al. oxide | Al. alloy |
| Young's modulus E ($N/m^2$) | 4.80E+10 | 2.00E+10 | 7.00E+10 | 4.00E+10 | 3.80E+11 | 1.00E+11 | 3.80E+11 | 7.00E+10 |
| Poisson ratio $\nu$ | 0.20 | 0.25 | 0.30 | 0.35 | 0.23 | 0.25 | 0.23 | 0.33 |
| Friction coefficient | 0.350 | 0.350 | 0.000 | 0.000 | 0.000 | 0.000 | 0.092 | 0.092 |
| Restitution coefficient | 1.00 | 1.00 | 1.00 | 1.00 | different values | | 0.98 | 0.98 |
| Density ($kg/m^3$) | 2800 | 2500 | 2699 | 1800 | 4000 | 7000 | 4000 | 2700 |
| Radius (m) | 0.010 | 0.010 | 0.100 | 0.100 | 0.0025 | 0.0025 | 0.0025 | 0.0025 |
| Velocity (m/s) | ±10 | ±10 | 0.2 | 0.2 | 3.9 | 3.9 | 3.9 | 3.9 |
| Input parameters | Test No.5 | | Test No.6 | | Test No.7 | | Test No.8 | |
| | Ex. 1 | Ex. 2 | Ex. 1 | Ex. 2 | Ex. 1 | Ex. 2 | Ex. 1 | Ex. 2 |
| | Steel | Polyethylene | Al. alloy | Nylon | Al. alloy | Copper | Al. alloy | Nylon |
| Young's modulus E ($N/m^2$) | 2.08E+11 | 1.00E+09 | 7.00E+10 | 2.50E+09 | 7.00E+10 | 1.20E+11 | 7.00E+10 | 2.50E+09 |
| Poisson ratio $\nu$ | 0.30 | 0.40 | 0.33 | 0.40 | 0.33 | 0.35 | 0.33 | 0.40 |
| Friction coefficient | 0.300 | 0.300 | 0.400 | 0.400 | 0.400 | 0.400 | 0.400 | 0.400 |
| Restitution coefficient | 1.00 | 1.00 | 0.50 | 0.50 | 0.50 | 0.50 | 0.50 | 0.50 |
| Density ($kg/m^3$) | 7850 | 1400 | 2700 | 1000 | 2700 | 8900 | 2700 | 1000 |
| Radius (m) | 1.00E–05 | 1.00E–05 | 0.100 | 0.100 | 0.100 | 0.100 | 0.100 | 0.100 |
| Velocity (m/s) | 5 | 5 | 0.2 | 0.2 | 0.2 | 0.2 | 0.2 | 0.2 |

*Al. alloy* Aluminum alloy, *Mg. alloy* Magnesium alloy, *Al. oxide* Aluminum oxide
Shear modulus G = E/2(1+v), NB = gravitational acceleration was set to zero

and contact damping. The contact damping is related to the coefficient of restitution. The computational time step was set at 1% of the Rayleigh critical time step [41,42] to ensure that the computational time step has negligible effect on the numerical outcomes. The corresponding input parameters for all benchmark tests are shown in Table 2. Each test has two

examples using different material properties so that the comparison of the impact response between different materials can be made. Several materials with different Young's moduli, Poisson's ratios and densities were used in the examples. These materials include steel, copper, aluminium alloy, magnesium alloy, aluminium oxide, glass, limestone, nylon, polyethylene and cast iron. The DEM results in these benchmark tests are compared with the analytical solutions described in the previous section and with experimental or FEA results found in the literature.

Test 1: Elastic normal impact of two identical spheres

Test 1 considers the simplest case of an elastic normal impact of two identical spheres with the same magnitude of velocity but in opposite directions. Two examples comprise glass and limestone respectively. The input parameters are listed in Table 2. The incoming velocity magnitude was set at 10 m/s. It is noted that the value of the restitution coefficient is unity for elastic normal impact.

The normal contact force is plotted against the normal contact displacement for glass and limestone spheres in Fig. 4a.

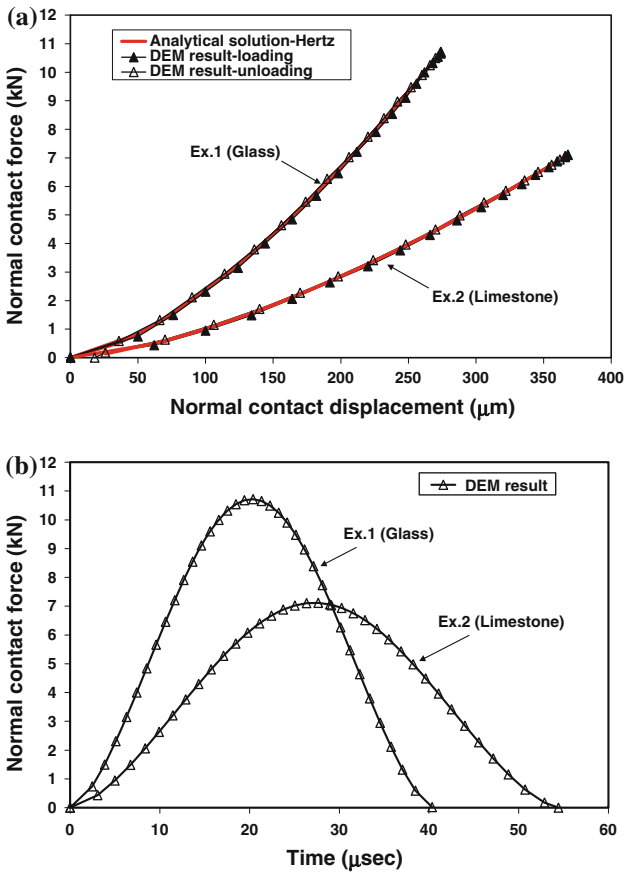


**Fig. 4** Test 1: elastic normal impact of two identical spheres: **a** force-displacement curve; **b** force-time curve

Both DEM results show that the unloading path of the FD curves is practically the same as the loading path, indicating that there is no energy dissipation when the restitution coefficient is unity. As expected, the FD curves of the DEM simulations using the Hertz–Mindlin contact model match with Hertz theory for elastic normal contact. The FD curve of limestone has a softer response than glass's as expected. Figure 4b shows the evolution of the normal contact force against time for both materials, which is symmetric for an elastic normal contact. The computed contact duration, maximum normal contact displacement and force in the two examples are compared with the analytical solutions (1–3) in Table 3. The discrepancies are all less than 0.1 %.

Test 2: Elastic normal impact of a sphere with a rigid plane

Test 2 considers an elastic normal impact between a sphere and a rigid plane. One example is for aluminium alloy and the other is for magnesium alloy. The input parameters are listed in Table 2. The incoming velocity was set at 0.2 m/s. The value of the restitution coefficient is also set to unity for elastic impact.

The computed force-displacement and force-time results for both materials are shown in Fig. 5. Both DEM results show no energy dissipation from the loading and unloading paths during the collision and match with Hertz theory. Aluminium alloy has a harder response than magnesium alloy. In the case of aluminium alloy, the FD curve obtained from Zhang and Vu-Quoc's finite element analysis [24] is also plotted and matches with the DEM result. The computed contact duration, maximum normal contact displacement and force in these two examples are compared with the analytical solutions ( 1–3) in Table 4. The discrepancies are all very small at less than 0.1 %.

Test 3: Normal contact with different restitution coefficients

Test 3 verifies the normal impact of a sphere on a rigid plane with different restitution coefficients (or different damping ratios). Two example calculations were performed for aluminium oxide and cast iron. The input values for the restitution coefficient were set at 0.0, 0.2, 0.4, 0.6, 0.8 and 1.0. Contact damping is the only source of energy dissipation due to normal impact. The incoming velocity was 3.9 m/s and the remaining input parameters are listed in Table 2. Figure 6 illustrates the comparison between the ratio of rebound velocity to impact velocity obtained from the computer simulations and the input value of the restitution coefficient for both materials. There is an exact agreement between the two, thus providing the verification that the DEM code is correct in this respect.

**Table 3** Comparison between DEM results and analytical solutions for elastic normal impact of two identical spheres

| Physical property | DEM result | | Analytical solution | | Difference (%) | |
|---|---|---|---|---|---|---|
| | Ex. 1 | Ex. 2 | Ex. 1 | Ex. 2 | Ex. 1 | Ex. 2 |
| Contact duration ($\mu$s) | 40 | 54 | 40 | 54 | 0.0 | 0.0 |
| Maximum displacement ($\mu$m) | 274 | 368 | 274 | 368 | 0.0 | 0.0 |
| Maximum force (N) | 10, 712 | 7, 113 | 10, 697 | 7, 108 | 0.1 | 0.1 |

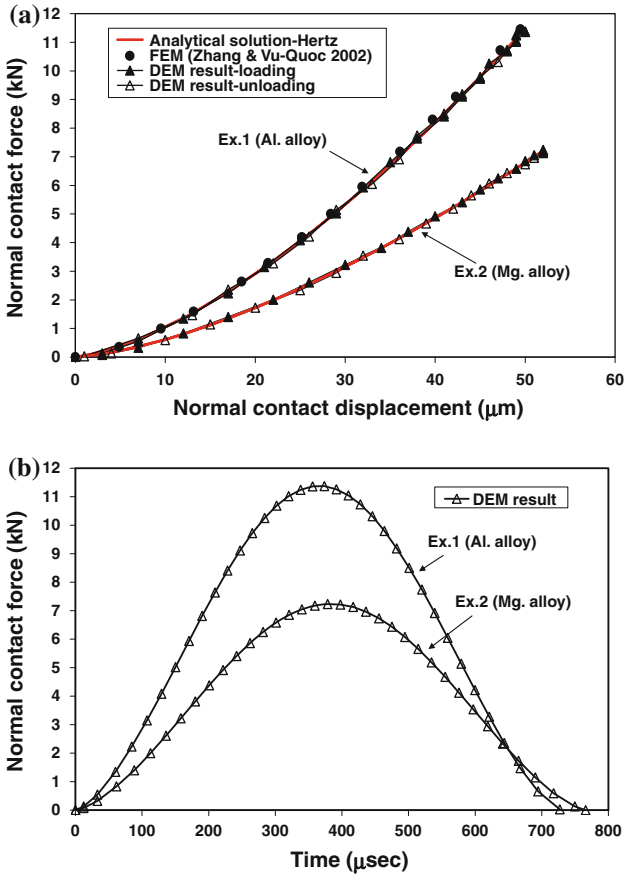


**Fig. 5** Test 2: elastic normal impact of a sphere with a rigid plane: **a** force-displacement curve; **b** force-time curve

Test 4: Oblique impact of a sphere with a rigid plane with a constant resultant velocity but at different incident angles

This test is to verify the case where a sphere impacts a rigid plane with a constant resultant velocity but at different incident angles, as shown in Fig. 7. Computations were performed for aluminium oxide and aluminium alloy. The constant velocity $V$ was set at 3.9 m/s and the incident angle was varied between 5° and 85°. The values for the restitution coefficient and friction coefficient were set to 0.98 and 0.092 respectively for the comparison with the experimental results from Kharaz et al. [30]. The input parameters are listed in Table 2.

Knowing that $V_{cn} = -V\cos\theta$ and $V_{ct} = V_{st} = V\sin\theta$, (24) can be rearranged as (29).

$$1 - \mu(1 + e_n)\cot\theta \leq e_t \tag{29}$$

Combining (19, 21, 23 and 26) and knowing that $\omega_1 = \omega_2 = \omega_2' = 0$, the post-collision angular velocity can be expressed as (30).

$$-\frac{5}{2}\frac{\mu(1 + e_n)V\cos\theta}{r_1} \leq \omega_1' \tag{30}$$

where the minus sign indicates that the sphere spins clockwise after impact. From (28), the recoil angle on the contact path $\varphi$ can be related to the incident angle $\theta$ as (31).

$$\tan^{-1}\left[\frac{\tan\theta}{e_n} - \frac{7}{2}\mu\left(1 + \frac{1}{e_n}\right)\right] \leq \varphi \tag{31}$$

The DEM results for the aluminium oxide are compared with the data obtained in the equivalent experiments (Kharaz et al. [30]) and the analytical solutions (29–31). Figure 8 shows the tangential coefficient of restitution based on the mass centre $e_t$ against the angle of incidence $\theta$. The DEM result matches the analytical solutions in both sliding and sticking regimes [as predicted by (29)]. The plot also shows good agreement with the experimental result except for incident angle less than 10°. This discrepancy in the sticking regime can be improved by using a more complete Hertz–Mindlin contact force model (Renzo and Maio [40]). Impact

**Table 4** Comparison between DEM results and analytical solutions for elastic normal impact of a sphere with a rigid plane

| Physical property | DEM result | | Analytical solution | | Difference (%) | |
|---|---|---|---|---|---|---|
| | Ex. 1 | Ex. 2 | Ex. 1 | Ex. 2 | Ex. 1 | Ex. 2 |
| Contact duration ($\mu$s) | 731 | 766 | 731 | 766 | 0.0 | 0.0 |
| Maximum displacement ($\mu$m) | 50 | 52 | 50 | 52 | 0.0 | 0.0 |
| Maximum force (N) | 11, 377 | 7, 235 | 11, 370 | 7, 233 | 0.1 | 0.0 |

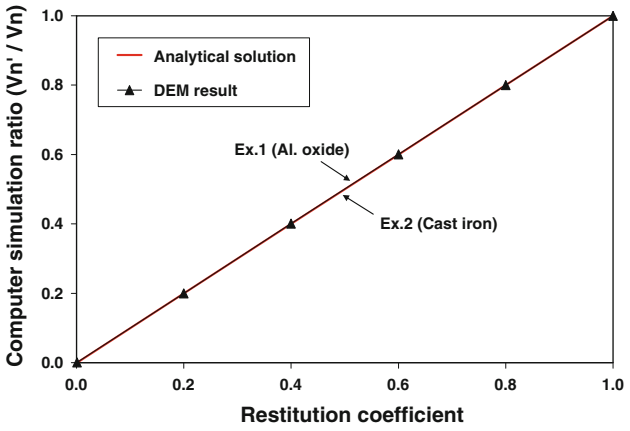


**Fig. 6** Test 3: comparison between simulated velocity ratio and input value of the restitution coefficient

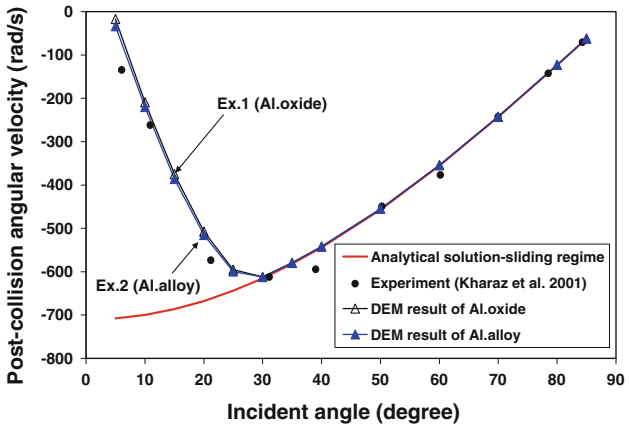


**Fig. 9** Test 4: simulated, theoretical and experimental post-collision angular velocity $\omega_1'$ for varying incident angles $\theta$

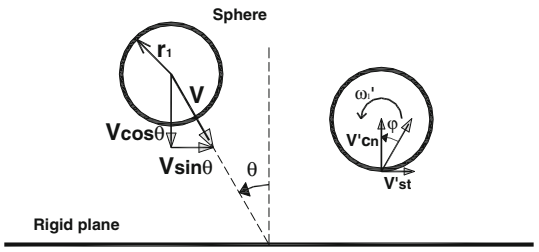


**Fig. 7** Test 4: a sphere impacting a rigid plane at incident angle $\theta$

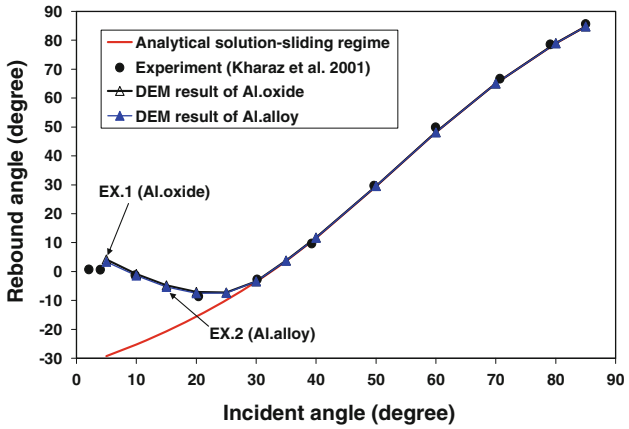


**Fig. 10** Test 4: simulated, theoretical and experimental rebound angles $\varphi$ for varying incident angles $\theta$

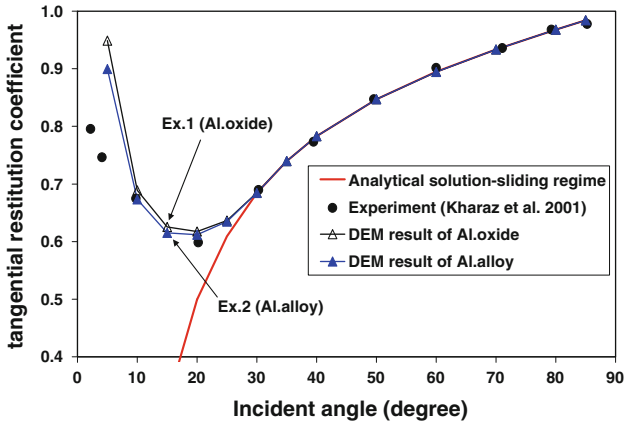


**Fig. 8** Test 4: simulated, theoretical and experimental tangential restitution coefficient $e_t$ for varying incident angles $\theta$

for incident angle greater than a critical value $\theta_{\text{critical}}$ can be expected to occur in sliding condition. Maw et al. [21] calculated this critical value to be approximately 28° when the restitution coefficient is unity. The DEM result predicted a value of 30° which is close to Maw et al.'s analytical solution: the small difference is due to a value of 0.98 for the restitution coefficient in both the DEM simulation and Kharaz et al.'s experiments.

The post-collision angular velocity $\omega_1'$ is plotted for various incident angles in Fig. 9. The DEM result matches the theoretical prediction given by (30) in sliding and sticking regimes and has an excellent agreement with Kharaz et al.'s experiments in both sliding and sticking regimes. A further indication is given in Fig. 10 which shows the predicted rebound angle against the incident angle. Again the DEM result follows the theoretical solution of (31) and gives an excellent match with the experimental data.

The DEM results for the second material (aluminium alloy) are also plotted in Figs. 8, 9, and 10. The results are in accordance with the analytical solutions in both sliding and sticking regimes [as predicted by (29–31)] and very close to those of aluminium oxide.

Test 5: Oblique impact of a sphere with a rigid plane with a constant normal velocity but at different tangential velocities

This test is to verify the case where a sphere impacts a rigid plane with a constant normal velocity but at different tangential velocities. One example is for steel and the other is for polyethylene. The constant normal velocity $V_n$ was set at 5 m/s and the tangential velocity $V_t$ was varied between 0.1 and 70.0 m/s. We consider an elastic oblique impact ($e_n = 1$) with friction as the only source of energy dissipation. The value for the friction coefficient was set to 0.3. The input parameters are listed in Table 2.

Giving that $V_{cn} = -V_n$, $V_{ct} = V_{st} = V_t$ and $e_n = 1$, (28) can be rewritten in a normalized form as (32).

$$\frac{V_t}{\mu V_n} - 7 \leq \frac{V'_{st}}{\mu V'_{cn}} \tag{32}$$

Similarly, combining (19, 21, 23 and 26) and knowing that $\omega_1 = \omega_2 = \omega'_2 = 0$, the post-collision angular velocity can be expressed as (33).

$$-5 \leq \frac{r_1 \omega'_1}{\mu V_n} \tag{33}$$

where the minus sign indicates that the sphere rotates clockwise after impact. The DEM results for steel were compared with the analytical solution by Maw et al. [21], FEA results by Wu et al. [25] and analytical solutions given in (32) and (33). The Poisson's ratio of the material in Maw et al.'s calculation was 0.3, as adopted in the DEM simulation. Wu et al. conducted a finite element analysis of an elastic oblique impact and the material properties in their calculation are the same as those adopted here except that the sphere was rigid and the substrate was elastic in their computation, whereas in the DEM computation, the sphere can "deform" locally by means of an overlap in the contact region and the wall is rigid. Figure 11a depicts the variation of the normalized recoil angle of the contact $\frac{V'_{st}}{\mu V'_{cn}}$ with the normalized incident angle $\frac{V_t}{\mu V_n}$. The DEM result agrees very well with all the three solutions in the sliding regime. However, there is some discrepancy in the sticking regime with the solutions from Maw et al. and Wu et al. with the DEM predicting smaller ratio of $\frac{V'_{st}}{\mu V'_{cn}}$. This is probably because the contact force model adopted in the DEM simulation is the widely used Hertz–Mindlin no-slip simplified model and not the complete theory of Hertz and Mindlin-Deresiewicz, as used in Maw et al.'s calculation. The normalized post-collision angular velocity $\left(\frac{r_1 \omega'_1}{\mu V_n}\right)$ is plotted against the normalized incident angle in Fig. 11b. The same observations can be made about the sliding regime, with DEM giving an excellent agreement with the FEA computation and the analytical solution given by (33), but producing some discrepancy in the sticking regime due to the

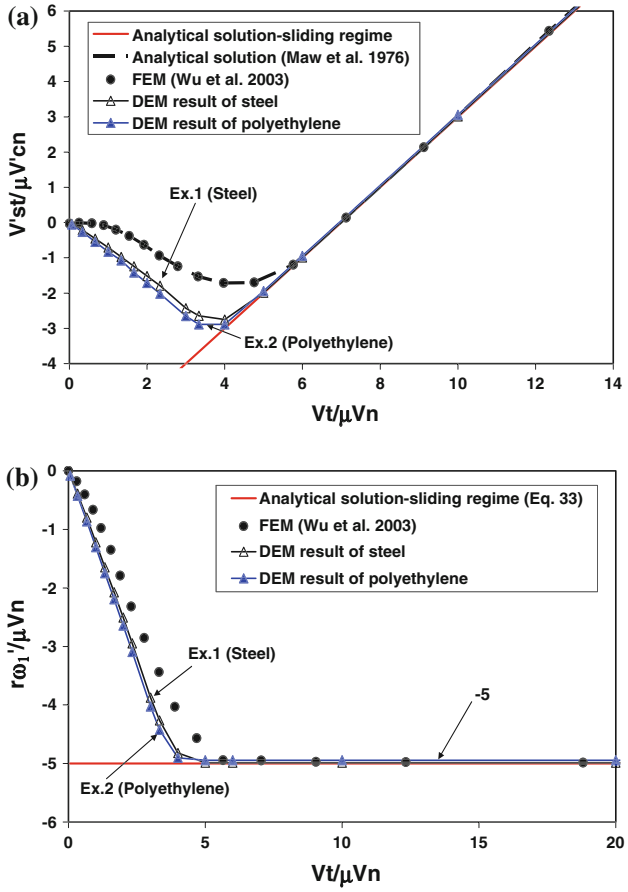


**Fig. 11** Test 5: oblique impact for varying tangential velocities: **a** normalized recoil angle versus normalized incident angle; **b** normalized post-collision angular velocity versus normalized incident angle

Hertz–Mindlin no-slip model employed in the DEM simulation. Again, this discrepancy between the DEM and FEA results in the sticking regime can be solved by using a more complete Hertz–Mindlin contact force model (Thornton et al. [43]).

The normalized recoil angle and post-collision angular velocity for polyethylene are also plotted against the normalized incident angle in the corresponding figures (Fig. 11a, b). These DEM results are in line with the analytical solutions (32–33) in both sliding and sticking regimes and give slightly smaller ratios of $\frac{V'_{st}}{\mu V'_{cn}}$ and $\frac{r_1 \omega'_1}{\mu V_n}$ than those for steel.

Test 6: Impact of a sphere with a rigid plane with a constant normal velocity but at different angular velocities

This test is to verify the case of oblique impact of a sphere on a rigid plane with a constant normal velocity but spinning at different angular velocities. One example is for aluminium alloy and the other is for nylon. The constant normal velocity $V_n$ was set at 0.2 m/s and the angular velocity $\omega_1$ (counterclockwise) was varied between 0.175 and 22.860 rad/s, which

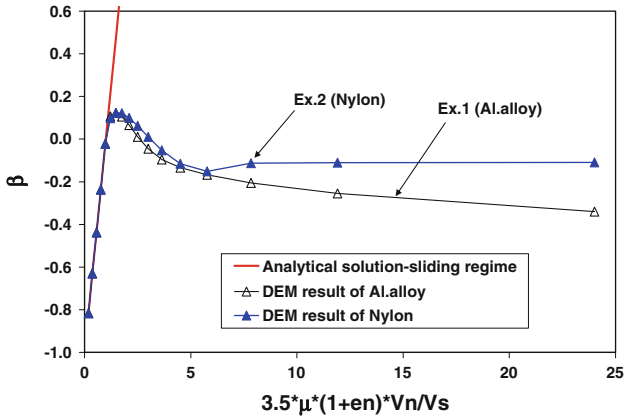


**Fig. 12** Test 6: oblique impact with different angular velocities: simulated and theoretical tangential restitution coefficient $\beta$ versus the quantity $\left[3.5\mu(1+e_n)\frac{V_n}{V_s}\right]$

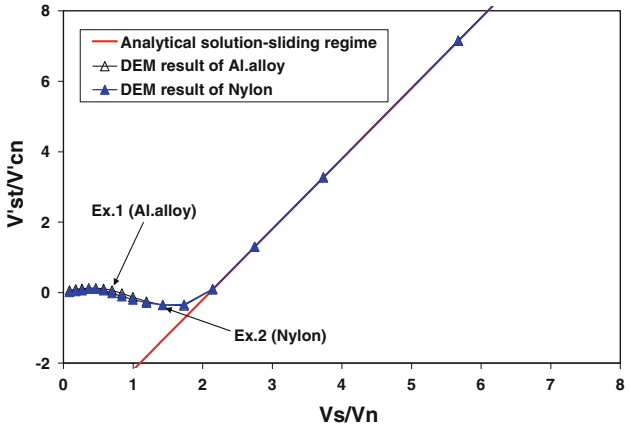


**Fig. 13** Test 6: simulated and theoretical tangent of recoil angle $\frac{V'_{st}}{V'_{cn}}$ for varying tangent of incident angles $\frac{V_s}{V_n}$

corresponds to the incident angle varying between 5° and 85°. Although the sphere approaches the rigid plane normally, it has a tangential velocity at the contact path due to the spin. The values for the restitution coefficient and friction coefficient were set to 0.5 and 0.4 respectively. The input parameters are listed in Table 2.

Knowing that $V_{cn} = -V_n$ and $V_{st} = r_1\omega_1 = V_s$, (26) can be rearranged as (34).

$$\beta \leq -1 + 3.5\mu(1+e_n)\frac{V_n}{V_s} \tag{34}$$

Similarly, (28) can be rearranged as (35).

$$-\frac{7}{2}\mu(1+\frac{1}{e_n}) + \frac{1}{e_n}\frac{V_s}{V_n} \leq \frac{V'_{st}}{V'_{cn}} \tag{35}$$

Figure 12 shows the DEM results of aluminium alloy and nylon for the variation of the tangential restitution coefficient $\beta$ (based on the contact path) with the quantity $3.5\mu(1+e_n)\frac{V_n}{V_s}$ and Fig. 13 depicts the variation of the tangent of recoil angle on the contact path $\frac{V'_{st}}{V'_{cn}}$ with the tangent of incident angle $\frac{V_s}{V_n}$ for both materials. It can be seen that for sliding collision, the tangential coefficient of restitution $\beta$ is a linear function of $\frac{V_n}{V_s}$ and that the tangent of the recoil angle $\frac{V'_{st}}{V'_{cn}}$ is also a linear function of the tangent of the corresponding incident angle $\frac{V_s}{V_n}$. These relationships in the two examples are as predicted theoretically by (34) and (35). Figure 12 also shows that there are two important parameters that control the collision regimes: the larger the friction coefficient $\mu$ and the ratio $\frac{V_n}{V_s}$, the more likely that the collision is sticking. It can be also seen from Figs. 12 and 13 that the tangential restitution coefficient for nylon is greater than that for aluminium alloy especially in the sticking regime, whilst the tangent of the recoil angle for nylon is almost the same as that for aluminium alloy.

Test 7: Impact of two identical spheres with a constant normal velocity and varying angular velocities

This test is to verify the case where two identical spheres collide with constant and opposite normal velocities and spinning at the velocities of the same magnitude but opposite direction. One example is for aluminium alloy and the other is for copper. The constant normal velocity was set at 0.2 m/s and the angular velocity was varied between 0.175 and 22.860 rad/s. The values for the restitution coefficient and friction coefficient were set to 0.5 and 0.4 respectively. The input parameters are listed in Table 2.

Since the relative pre-collision tangential velocity on the contact path is zero, no tangential force is generated during this normal impact, i.e. $f_t = 0$ and $F_t = 0$. Knowing that $V_{ct,1} = V_{ct,2} = 0$, we can deduce from (7) and (10) that the recoil tangential velocities

$$V'_{ct,1} = V'_{ct,2} = 0 \tag{36}$$

Similarly, from (9) and (12), we can deduce that the recoil angular velocities

$$\omega'_1 = \omega_1; \omega'_2 = \omega_2 \tag{37}$$

Figure 14 shows the post-collision tangential velocity of Sphere 1 or Sphere 2 at the mass centre against varying pre-collision angular velocities for both materials. The DEM results show that the post-collision tangential velocity of Sphere 1 or Sphere 2 at the mass centre is zero, which matches the analytical solution given by (36). The post-collision angular velocity of Sphere 1 or Sphere 2 for both materials is plotted against the pre-collision angular velocity in Fig. 15, showing that the DEM results follow exactly the analytical prediction given by (37).

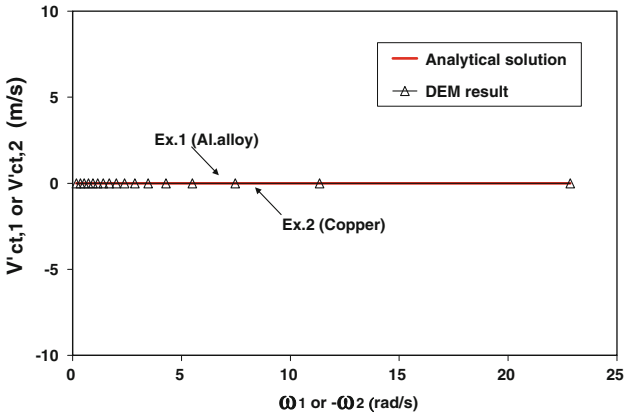


**Fig. 14** Test 7: post-collision tangential velocity at the mass centre for varying pre-collision angular velocities

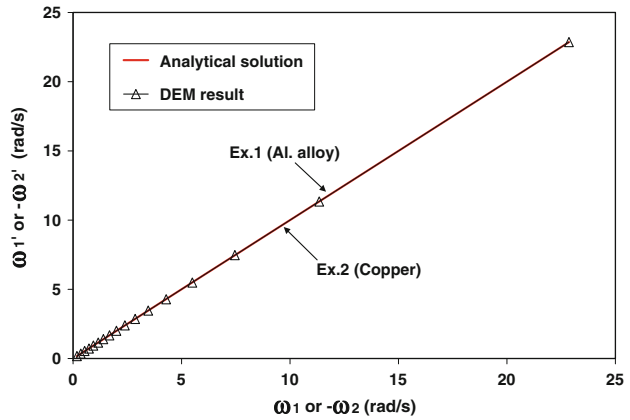


**Fig. 15** Test 7: post-collision angular velocity for varying pre-collision angular velocities

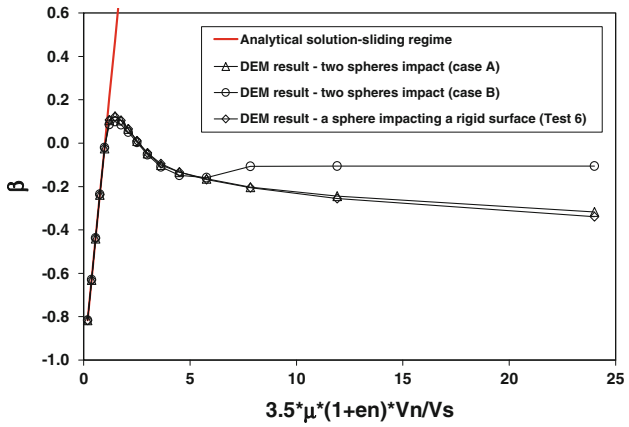


**Fig. 16** Test 8 (Ex.1. Al. alloy): simulated and theoretical tangential restitution coefficient $\beta$ versus quantity $\left[3.5\mu(1+e_n)\frac{V_n}{V_s}\right]$

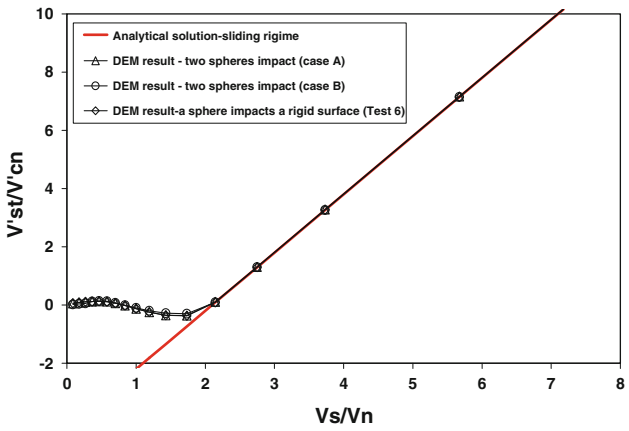


**Fig. 17** Test 8 (Ex.1. Al. alloy): simulated and theoretical tangent of recoil angle $\frac{V'_{st}}{V'_{cn}}$ versus tangent of incident angle $\frac{V_s}{V_n}$ for the small sphere

Test 8: Impact of two differently sized spheres with a constant normal velocity and varying angular velocities

This test is to verify the case where a small sphere with a constant normal velocity but at different angular velocities collides with a big sphere which is stationary before collision. One example is for aluminium alloy and the other is for nylon. The density of the big sphere was 1,000 times that for the small sphere and the radius of the big sphere was 5 times that for the small sphere. The constant normal velocity was 0.2 m/s and the angular velocity was varied between 0.175 and 22.860 rad/s. The values for the restitution coefficient and friction coefficient were set to 0.5 and 0.4 respectively. The input parameters for the small sphere are listed in Table 2.

We consider the following two cases: (A) the shear modulus of the big sphere is 1,000 times that for the small sphere; and (B) the big sphere has the same mechanical properties as the small sphere. The DEM results of Case A and Case B for the two materials were compared to the analytical solutions given by (34) and (35), which are also valid for this test. The result for Test 6 where a sphere impacts a rigid plane with a constant normal velocity but at different angular velocities, using the same input parameters as those for the small sphere, is also shown for comparison.

Figure 16 shows the variation of the tangential restitution coefficient based on the contact path $\beta$ with the quantity $\left[3.5\mu(1+e_n)\frac{V_n}{V_s}\right]$ for aluminium alloy. The variation of the tangent of recoil angle on the contact path against the tangent of incident angle for the small sphere in the case of aluminium alloy is plotted in Fig. 17. The DEM results of Case A and Case B match with the analytical solutions (34 and 35) in both sliding and sticking regimes. The match between Case A and Test 6 can be expected since a big sphere with a very large mass and stiffness would serve as a rigid plane, which is equivalent to the case in Test 6.

For nylon, the tangential restitution coefficient $\beta$ is plotted against the quantity $\left[3.5\mu(1+e_n)\frac{V_n}{V_s}\right]$ in Fig. 18 and the tangent of recoil angle for the small sphere is plotted against

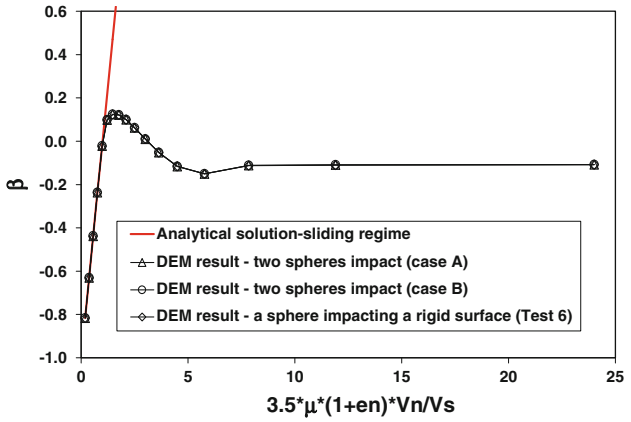


**Fig. 18** Test 8 (Ex.2. Nylon): simulated and theoretical tangential restitution coefficient $\beta$ versus quantity $\left[3.5\mu(1+e_n)\frac{V_n}{V_s}\right]$

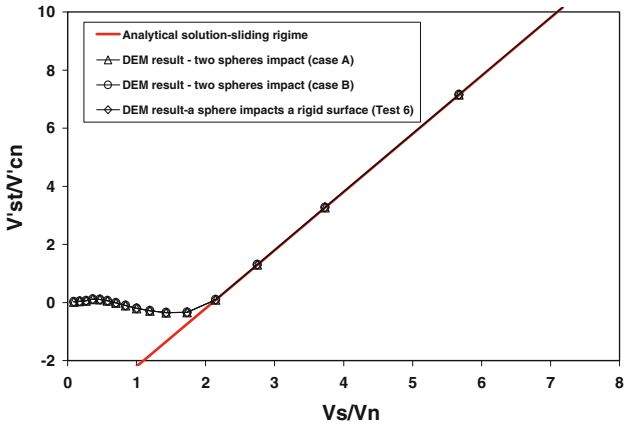


**Fig. 19** Test 8 (Ex.2. Nylon): simulated and theoretical tangent of recoil angle $\frac{V'_{st}}{V'_{cn}}$ versus tangent of incident angle $\frac{V_s}{V_n}$ for the small sphere

the tangent of incident angle in Fig. 19. Figures 18 and 19 show that the DEM results for Case A and Case B are in agreement with the analytical solutions (34–35) in both sliding and sticking regimes and the DEM results for three cases (Case A, Case B and Test 6) are almost identical for nylon.

## 4 Conclusion

A set of benchmark tests has been proposed for verifying DEM codes at particle impact level. The analytical solutions obtained from elasticity theory for elastic normal impact between two spheres or a sphere with a rigid plane have been reviewed. The analytical solutions for frictional oblique impact of two spheres or a sphere with a rigid plane have been examined and derived. This simple mathematical model assumes the restitution coefficient to be a constant. The pre-collision and post-collision velocities predicted by any DEM contact force model should satisfy these analytical solutions. These benchmark tests were then demonstrated using the PFC3D and EDEM commercial codes and explored to comprehend the fundamental impact phenomena. Test 1 and Test 2 are restricted to the elastic regime for normal impact, whilst the other tests (Test 3–Test 8) describe the energy dissipation due to the collision of two spheres or a sphere with a rigid plane. The DEM results in these benchmark tests have been compared with the analytical solutions and the experimental or FEA results found in the literature.

All benchmark tests showed good to excellent match, providing a quantitative verification for the PFC3D and EDEM codes. Some minor discrepancies in the sticking regime have been noted which are attributed to the adopted contact force model and can be resolved using a more complete Hertz–Mindlin contact force model. This gives some confidence in the use of these codes although it should be borne in mind that large scale DEM simulations have many further challenges to overcome. The analytical solutions provide a useful insight into particle impact mechanics and guidance on the suitability of the discrete element method for modelling various particle scale phenomena. The DEM results also supplement further information on some aspects in the sticking regime for frictional oblique impact, where the analytical solutions can only provide an upper bound. These benchmark tests not only verify DEM codes but also enhance the understanding of fundamental impact phenomena.

## References

1. Cundall, P.A., Strack, O.D.L.: Discrete numerical-model for granular assemblies. Geotechnique **29**, 47–65 (1979)
2. Zhu, H.P., Yu, A.B., Wu, Y.H.: Numerical investigation of steady and unsteady state hopper flows. Powder Technol. **170**, 125–134 (2006)
3. Ketterhagen, W.R., Curtis, J.S., Wassgren, C.R., Hancock, B.C.: Predicting the flow mode from hoppers using the discrete element method. Powder Technol. **195**, 1–10 (2009)
4. Tao, H., Baosheng, J., Zhong, W.Q, Wang, X.F., Ren, B., Zhang, Y., Xiao, R.: Discrete element method modeling of non-spherical granular flow in rectangular hopper. Chem. Eng. Process. **49**, 151–158 (2010)
5. Kwan, C.C., Mio, H., Chen, Y.Q., Ding, Y.L., Saito, F., Papadopoulos, D.G., Bentham, A.C., Ghadiri, M.: Analysis of the milling rate of pharmaceutical powders using the Distinct Element Method (DEM). Chem. Eng. Sci. **60**, 1441–1448 (2005)
6. Yang, R.Y., Jayasundara, C.T., Yu, A.B., Curry, D.: DEM simulation of the flow of grinding media in IsaMill. Miner. Eng. **19**, 984–994 (2006)
7. Cleary, P.W., Sinnott, M.D., Morrison, R.D.: DEM prediction of particle flows in grinding processes. Int. J. Numer. Methods Fluids **58**, 319–353 (2008)
8. Müller, C.R., Holland, D.J., Sederman, A.J., Scott, S.A., Dennis, J.S., Gladden, L.F.: Granular temperature: comparison of magnetic resonance measurements with discrete element model simulations. Powder Technol. **184**, 241–253 (2008)

9. Chu, K.W., Wang, B., Yu, A.B., Vince, A.: CFD-DEM modelling of multiphase flow in dense medium cyclones. Powder Technol. **193**, 235–247 (2009)
10. Maio, F.P.D., Renzo, A.D., Trevisan, D.: Comparison of heat transfer models in DEM-CFD simulations of fluidized beds with an immersed probe. Powder Technol. **193**, 257–265 (2009)
11. Lu, L.S., Hsiau, S.S.: Mixing in a vibrated granular bed: diffusive and convective effects. Powder Technol. **184**, 31–43 (2008)
12. Majid, M., Walzel, P.: Convection and segregation in vertically vibrated granular beds. Powder Technol. **192**, 311–317 (2009)
13. Naeini, S.E., Spelt, J.K.: Two-dimensional discrete element modeling of a spherical steel media in a vibrating bed. Powder Technol. **195**, 83–90 (2009)
14. Luding, S.: Cohesive, frictional powders: contact models for tension. Granul. Matter **10**, 235–246 (2008)
15. Härtl, J., Ooi, J.Y.: Experiments and simulations of direct shear tests: porosity, contact friction and bulk friction. Granul. Matter **10**, 263–271 (2008)
16. Chung, Y.C., Ooi, J.Y.: A study of influence of gravity on bulk behaviour of particulate solid. Particuology **6**, 467–474 (2008)
17. Holst, J.M.F.G., Ooi, J.Y., Rotter, J.M., Rong, G.H.: Numerical modeling of silo filling. I: continuum analyses. J. Eng. Mech. **125**, 94–103 (1999)
18. Holst, J.M.F.G., Rotter, J.M., Ooi, J.Y., Rong, G.H.: Numerical modeling of silo filling. II: discrete element analyses. J. Eng. Mech. **125**, 104–110 (1999)
19. Timoshenko, S.P., Goodier, J.N.: Theory of Elasticity. 3rd edn. McGraw-Hill, New York (1970)
20. Hertz, H.: Miscellaneous Papers. McMillan, New York (1896)
21. Maw, N., Barber, J.R., Fawcett, J.N.: The oblique impact of elastic spheres. Wear **38**, 101–114 (1976)
22. Mindlin, R.D., Deresiewicz, H.: Elastic spheres in contact under varying oblique forces. J. Appl. Mech. (Trans. ASME) **20**, 327–344 (1953)
23. Vu-Quoc, L., Zhang, X., Lesburg, L.: Normal and tangential force-displacement relations for frictional elasto-plastic contact of spheres. Int. J. Solids Struct. **38**, 6455–6489 (2001)
24. Zhang, X., Vu-Quoc, L.: Modeling the dependence of the coefficient of restitution on the impact velocity in elasto-plastic collisions. Int. J. Impact Eng. **27**, 317–341 (2002)
25. Wu, C.Y., Thornton, C., Li, L.Y.: Coefficients of restitution for elastoplastic oblique impacts. Adv. Powder Technol. **14**, 435–448 (2003)
26. Vu-Quoc, L., Zhang, X.: An elastoplastic contact force-displacement model in the normal direction: displacement-driven version. Proc. R. Soc. Lond. Ser. A **455**, 4013–4044 (1999)
27. Vu-Quoc, L., Lesburg, L., Zhang, X.: An accurate tangential force-displacement model for granular-flow simulations: contacting spheres with plastic deformation, force-driven formulation. J. Comput. Phys. **196**, 298–326 (2004)
28. Zhang, X., Vu-Quoc, L.: An accurate elasto-plastic frictional tangential force-displacement model for granular flow simulations: displacement-driven formulation. J. Comput. Phys. **225**, 730–752 (2007)
29. Foerster, S.F., Louge, M.Y., Chang, H., Allia, K.: Measurements of the collision properties of small spheres. Phys. Fluids **6**, 1108–1115 (1994)
30. Kharaz, A.H., Gorham, D.A., Salman, A.D.: An experimental study of the elastic rebound of spheres. Powder Technol. **120**, 281–291 (2001)
31. Plantard, G., Papini, M.: Mechanical and electrical behaviors of polymer particles: Experimental study of the contact area between two particles.Experimental validation of a numerical model. Granul. Matter **7**, 1–12 (2005)
32. Tsuji, Y., Tanaka, T., Ishida, T.: Lagrangian numerical-simulation of plug flow of cohesionless particles in a horizontal pipe. Powder Technol. **71**, 239–250 (1992)
33. Itasca Consulting Group Inc. PFC3D–Particle Flow Code in Three Dimensions, Version 3.0. Minneapolis, USA (2003)
34. DEM Solutions Ltd. EDEM Discrete Element Code, Beta Version. Edinburgh, UK (2005). (http://www.dem-solutions.com/)
35. Chung,Y.C.: Discrete element modelling and experimental validation of a granular solid subject to different loading conditions. PhD Thesis, University of Edinburgh, Edinburgh, UK (2006)
36. Walton, O.R: Numerical simulation of inelastic, frictional particle–particle interactions. In: Roco, M.C. (ed.) Particulate Two-Phase Flow, pp. 884–911. Butterworth-Heinemann, Boston (1993)
37. Vu-Quoc, L., Zhang, X.: An accurate and efficient tangential force-displacement model for elastic frictional contact in particle-flow simulations. Mech. Mater. **31**, 235–269 (1999)
38. Meriam, J.L., Kraige, L.G.: Engineering Mechanics-Dynamics. Wiley, New York (2003)
39. Ning, Z., Ghadiri, M.: Incorporation of Rayleigh damping into TRUBAL and determination of the critical time step. (1996)
40. Renzo, A.D., Maio, F.P.D.: Comparison of contact-force models for the simulation of collisions in DEM-based granular flow codes. Chem. Eng. Sci. **59**, 525–541 (2004)
41. Johnson, K.L.: Contact Mechanics. Cambridge University Press, Cambridge (1985)
42. Thornton, C., Randall, C.W. : Applications of theoretical contact mechanics to solid particle system simulation. In: Satake, M., Jenkins, J.T. (eds.) Micromechanics of Granular Materials, pp. 133–142. Elsevier, Amsterdam (1988)
43. Thornton, C., Ning, Z., Wu, C.Y., Nasrullah, M., Li, L.Y.: Contact mechanics and coefficients of restitution. In: Poschel, T., Luding, S. (eds.) Granular Gases, pp. 55–66. Springer, Berlin (2001)